MicroRNA-155 regulates osteogenesis and bone mass phenotype via targeting S1PR1 gene

Zhichao Zheng[1, 2,#], Lihong Wu[1,#], Zhicong Li[1,#], Ruoshu Tang[1], Hongtao Li[3], Yinyin Huang[1], Zhitong Ye[1], Dong Xiao[4,5], Xiaolin Lin[4,5], Gang Wu[6, 7]*, Richard T Jaspers[2,*], Janak L. Pathak[1,*]

[1]Affiliated Stomatology Hospital of Guangzhou Medical University, Guangdong Engineering Research Center of Oral Restoration and Reconstruction, Guangzhou Key Laboratory of Basic and Applied Research of Oral Regenerative Medicine, Guangzhou, Guangdong 510182, China

[2]Laboratory for Myology, Department of Human Movement Sciences, Faculty of Behavioural and Movement Sciences, Vrije Universiteit Amsterdam, Amsterdam Movement Sciences, Amsterdam 1081 HZ, The Netherlands

[3]State Key Laboratory of Respiratory Diseases, National Clinical Research Center for Respiratory Diseases, Guangzhou Institute of Respiratory Health, the First Affiliated Hospital of Guangzhou Medical University, Guangzhou, Guangdong 510230, China

[4]Guangdong Provincial Key Laboratory of Cancer Immunotherapy Research and Guangzhou Key Laboratory of Tumour Immunology Research, Cancer Research Institute, School of Basic Medical Science, Southern Medical University, Guangzhou 510515, China

[5]Institute of Comparative Medicine & Laboratory Animal Center, Southern Medical University, Guangzhou 510515, China

[6]Department of Oral and Maxillofacial Surgery/Pathology, Amsterdam UMC and Academic Center for Dentistry Amsterdam (ACTA), Amsterdam Movement Science, Vrije Universiteit Amsterdam, Amsterdam, the Netherlands.

[7]Department of Oral Cell Biology, Academic Center for Dentistry Amsterdam (ACTA), University of Amsterdam and Vrije Universiteit Amsterdam, Amsterdam, the Netherlands.

[#]These authors contributed equally to this work

***** Corresponding authors

Janak L. Pathak,

Email: j.pathak@gzhmu.edu.cn

Richard T Jaspers

Email: r.t.jaspers@vu.nl

Gang Wu

Email: g.wu@acta.nl

Abstract

MicroRNA-155 (miR155) is overexpressed in various inflammatory diseases and cancer, in which bone resorption and osteolysis are frequently observed. However, the role of miR155 on osteogenesis and bone mass phenotype is still unknown. Here, we report a low bone mass phenotype in the long bone of miR155-Tg mice compared with control mice. In contrast, miR155-KO mice showed a high bone mass phenotype. miR155-KO mice showed robust bone regeneration in the ectopic and orthotopic model, but miR155-Tg mice showed compromised bone regeneration compared with the control mice. Similarly, the osteogenic differentiation potential of bone marrow stromal stem cells (BMSCs) from miR155-KO mice was robust and miR155-Tg was compromised compared with that of control mice. Moreover, miR155 knockdown in BMSCs from control mice showed higher osteogenic differentiation potential, supporting the results from miR155-KO mice. TargetScan analysis predicted S1PR1 as a target gene of miR155, which was further confirmed by luciferase assay and miR155 knockdown. S1PR1 overexpression in BMSCs robustly promoted osteogenic differentiation without affecting cell viability and proliferation. Thus, miR155 showed a catabolic effect on osteogenesis and bone mass phenotype via interaction with the S1PR1 gene, suggesting inhibition of miR155 as a potential strategy for bone regeneration and bone defect healing.

Keywords: miR155, osteogenesis, bone mass phenotype, S1PR1, cell viability

Introduction

MicroRNAs (miRNAs) are a class of endogenous non-coding RNAs with 18-22 nucleotides length that bind to the 3′-untranslated region of the target gene and regulate the target gene expression (1). miRNAs regulate cell functions such as growth, differentiation, and energy metabolism by silencing the target gene via degradation or translational repression (1, 2). Moreover, miRNAs are also involved in the pathophysiology of various inflammatory diseases and cancers (3-5). Certain miRNAs had been reported to regulate osteogenesis and bone homeostasis (5, 6). MicroRNA-155 (miR155) is one of the best conserved and multifunctional miRNAs that regulate several biological processes and diseases such as tumorigenesis, cardiovascular disease, kidney diseases, etc (7-10). miR155 is upregulated in inflammatory diseases and cancers, including periodontitis, lung cancer, liver cancer, and breast cancer (11-14). Systemic bone loss is frequently observed in patients with inflammatory diseases and cancers (15, 16). However, the role of miR155 on osteogenesis and bone homeostasis is still unclear.

Induced osteoclasts formation/activity and compromised osteogenic differentiation disrupt bone homeostasis causing bone loss (17, 18). Osteoclasts formation and activity are induced during inflammation and cancer (19, 20). miR155 had been reported to induce osteoclastogenesis (21). miR155 knockout (miR155-KO) mice exhibit reduced local bone destruction in arthritis attributed to reduced generation of osteoclasts (22). Osteogenic differentiation of precursor cells results in bone formation and is the key anabolic event of bone homeostasis. Reduced osteogenic differentiation of precursor cells causes low bone mass phenotype increasing the risk of fracture. Osteogenesis is also a key biological process of bone tissue engineering. Various miRNAs targeted approaches had been developed to promote bone regeneration and bone defect healing during bone tissue engineering (23). The role of miR155 on osteogenic differentiation and bone regeneration is rarely investigated. Compromised osteogenesis and low bone mass phenotype are frequently observed in patients with inflammatory diseases and cancers (24, 25). Similarly, effective bone

regeneration and bone defect healing are also key challenges in patients with inflammatory diseases. miR155 targets multiple genes to regulate the pathophysiology of a specific disease in a cell-type-specific manner (26). Sphingosine 1-phosphate receptor-1 (S1PR1) is one of the target genes of miR155 (27), which has been reported to positively regulate osteogenic differentiation of precursor cells (28, 29). Therefore, it is wise to explore the involvement of S1PR1 in miR155-mediated effect on osteogenesis.

In this study, we aimed to analyze the effect of different levels of miR155 on osteogenesis and bone mass phenotype using miR155 transgenic (miR155-Tg) and miR155-KO mice. This study also investigated the role of miR155 target gene S1PR1 on osteogenic differentiation of BMSCs. We found a catabolic effect of miR155 on osteogenesis and bone mass phenotype via targeting the S1PR1 gene.

Results

miR155-Tg mice showed a low bone mass phenotype

Micro-CT images showed fewer and thinner trabeculae in miR155-Tg mice femur compared to control mice (Fig. 1A). Trabecular bone parameter BV/TV, BMD, Tb.N, and Tb.Th were significantly reduced in miR155-Tg mice compared to control mice (Fig. 1B-1E). In miR155-Tg mice Tb.Sp was significantly increased compared to control mice (Fig. 1F). These results indicate the low bone mass phenotype in miR155-Tg mice.

miR155-KO mice showed a high bone mass phenotype

Micro-CT images showed robustly dense and interconnected trabeculae in miR155-KO mice compared to control mice (Fig. 2A). The trabecular bone parameters BV/TV, BMD, Tb.N in miR155-KO mice were 2-, 2.69-, 1.83-, respectively, compared to control mice (Fig. 2B-2D). While Tb.Th was not significantly changed (Fig. 2E). Tb.Sp in miR155-KO mice was significantly reduced

compared to control mice (Fig. 2F). These results indicate the high bone mass phenotype of miR155-KO mice. miR155-KO and miR155-Tg showed an opposite trend of bone mass phenotype and trabecular bone parameters (Fig. 1 and 2), suggesting the role of miR155 in bone homeostasis regulation.

Ectopic bone regeneration was inhibited in miR155-Tg mice while increased in miR155-KO mice

A bone regeneration study was conducted to investigate whether the bone regeneration potential is altered in miR155-Tg and miR155-KO mice. BMP2-loaded collagen membranes were implanted in mice ectopically to confirm the bone regeneration potential in the ectopic site of miR155-Tg, miR155-KO, and control mice. Micro-CT images showed very less bone volume in collagen membrane transplanted in miR155-Tg mice compared to that of control mice (Fig. 3A). The miR155-Tg group showed significantly reduced BV/TV and Tb.N in newly formed bone compared to the control group (Fig. 3B). Tb.Sp was increased in the miR155-Tg group compared to the control group (Fig. 3B). In contrast, ectopic bone regeneration was significantly increased in the miR155-KO group compared to the control group (Fig. 3C). Newly formed bone BV/TV and Tb.N in the miR155-KO group were increased by 6.12-, and 5.64-fold respectively compared to the control group (Fig. 3D). The Tb.Sp was significantly reduced in the miR155-KO group compared control group (Fig. 3J). These results indicate a catabolic effect of miR155 on bone regeneration.

miR155-KO mice showed enhanced bone regeneration in an orthotopic model

To further confirm the catabolic effect of miR155 on bone regeneration, we adopted a calvarial bone defect healing model in miR155-KO mice. Micro-CT images showed more newly formed bone in the defect area of the miR155-KO group compared to the control group (Fig. 4A). Newly formed bone parameter analysis showed higher BV/TV (3.49-fold), and Tb.N (2.85-fold) in the miR155-KO group compared to the

control group (Fig. 4B and 4C). There was no significant difference in Tb.Th and Tb.Sp between the groups (Fig. 4D, 4E). These results indicate the anabolic effect of miR155 knockout on bone regeneration.

miR155 influences the osteogenic differentiation of BMSCs

To further confirm the regulatory role of miR155 on osteogenesis, we analyzed the osteogenic differentiation potential BMSCs isolated from miR155-Tg, miR155-KO, and control mice. Mineralized matrix deposition potential in BMSCs from miR155-TG mice was prominently reduced compared to control mice (Fig. 5A and 5B). Similarly, protein level expressions of osteogenic markers ALP and Runx2 in BMSCs from R155-Tg mice were reduced compared to that of control mice (Fig. 5C). These results indicate the compromised osteogenic differentiation potential of BMSCs from miR155-Tg mice. In contrast, BMSCs from miR155-KO mice showed robustly higher matrix mineralization potential compared to that of control mice (Fig. 5D and 5E). The protein level expressions of osteogenic markers ALP were enhanced in BMSCs from miR155-KO (Fig. 5F). These results demonstrated the catabolic effect of miR155 in osteogenic differentiation.

Knockdown of miR155 induced osteogenic differentiation of BMSCs

Matrix mineralization was robustly increased in the miR155 sponge group compared to the negative control group (Fig. 6A and 6B). miR155 was knockdown in BMSCs to further confirm the role of miR155 level in osteogenic differentiation. miR155 sponge lentivirus treatment significantly reduced the expression of miR155 in BMSCs (Fig. 6C), indicating the successful knockdown of miR155. Similarly, the protein level expression of osteogenic markers ALP and Runx2 was robustly upregulated in the miR155 sponge group compared to the negative control group (Fig. 6E). These results showed a catabolic effect of miR155 on osteogenic differentiation of precursor cells.

miR155 targets the S1PR1 gene to regulate osteogenic differentiation of BMSCs.

TargetScan predicted S1PR1 as a target gene of miR155 (Fig. 7A). Luciferase reporter gene assay was performed to analyze the miR155 and S1PR1 gene interaction (Fig. 7B). Our results showed that miR155 directly binds to the 3'UTR of the S1PR1 (Fig. 7B). miR155 robustly enhanced the protein level expression of the S1PR1 gene in BMSCs (Fig. 7C), confirming the interaction of miR155 and the S1PR1 gene. S1PR1 transfection in BMSCs robustly enhanced the matrix mineralization (Fig. 7D and 7E). The protein level expression of S1PR1 was enhanced in lentivirus-mediated S1PR1 overexpressed BMSCs (Fig, 7F). This result indicates the efficacy of lentivirus-based S1PR1 overexpression in BMSCs. The protein level expression of ALP and Runx2 was increased in S1PR1 overexpressed BMSCs (Fig. 7F). S1PR1 overexpression in BMSCs by lentivirus did not affect cell viability and proliferation (Fig. 7G). These results indicate that the miR155 targets the S1PR1 gene to regulate osteogenic differentiation of BMSCs.

Discussion

Differentiation of mesenchymal stem cells to osteoblasts is a vital event of bone regeneration. Differentiated osteoblasts deposit mineralized matrix and contribute to new bone formation. Various miRNAs had been reported to regulate osteogenesis and bone mass phenotype (23). In this study, miR155-Tg mice showed compromised bone regeneration and low bone mass phenotype. In contrast, miR155-KO mice showed improved bone regeneration and a higher bone mass phenotype. BMSCs from miR155-Tg and miR155-KO mice showed compromised and robust osteogenic differentiation potential, respectively. miR155 silencing also promoted osteogenic differentiation potential in BMSCs. These results indicate a catabolic effect of miR155 on bone regeneration and bone mass phenotype. Knockdown of miR155 in BMSCs robustly enhanced the protein level expression of S1PR1 and osteogenic regulator Runx2, indicating S1PR1 as a target gene of miR155 in BMSCs to regulate osteogenic differentiation. S1PR1 overexpression in BMSCs enhanced Runx2 expression and osteogenic differentiation of BMSCs indicating the regulatory role of

miR155-S1PR1 interaction on osteogenesis (Fig. 8).

miRNAs/anti-miRNAs have been used for bone tissue engineering (23). MiR26a (30), anti-miR31 (31), anti-miR34a (32), miR135 (33), anti-miR138 (34), anti-miR146a (35), miR148a (36), anti-miR221 (37), anti-miR-3555p (38) had shown anabolic effect on osteogenic differentiation of precursor cells and bone defect healing. Most of the miRNAs/anti-miRNAs promote bone regeneration via activation of osteogenic master regulator Runx2 (23). In this study, miR155 overexpression showed a catabolic effect on osteogenesis and bone mass phenotype. Interestingly, knockout or knockdown of miR155 showed an anabolic effect on osteogenesis and bone defect healing. Runx2 was involved in the miR155-mediated regulation of osteogenic differentiation of BMSCs. miR155 had been reported to inhibit osteogenesis of MC3T3-E1 cells via SMAD5 downregulation (39). miR155 inhibits BMP9-induced osteogenic differentiation of precursor cells via downregulation of BMP signaling (40). Qu et al. revealed the miR155 inhibition could alleviate suppression of the osteogenic differnentiation of human BMSCs under the condition of under high glucose and free fatty acids by targeting SIRT1 (41). Our results from miR155-Tg mice on inhibition of osteogenesis are in accordance with the findings from the literature (39, 40). To our knowledge, this is the first study to report the anabolic effect of miR155 knockout or knockdown on osteogenic differentiation of precursor cells. Our results suggest the potential application of anti-miR155 on bone regeneration and bone tissue engineering application.

Anti-miR155 oligonucleotides and antagomir have been designed for various cancer treatments (42, 43). Small molecule-based cyclic peptidomimetics had shown an inhibitory effect on miR155 biogenesis(44). MLN4924 is an inhibitor of the NEDD8-activating enzyme. MLN4924 decreases the binding of NF-κB to the miR155 promoter and downregulates miR155 in AML cells (45). Since, knockdown of miR155 robustly promoted the osteogenesis and bone mass phenotype, anti-miR155 or miR155 inhibitor could apply for bone tissue engineering application as well as the treatment of low bone mass phenotype. However, the osteoinductive potential of

already available anti-miR155 or miR155 inhibitors should be tested using in vitro and in vivo models to prove this hypothesis.

miR155 targets different genes in different cells to regulate the cell type-specific functions (46-49). S1PR1, a target gene of miR155, is regulated during various physiological and pathological conditions (49, 50). In this study, miR155 inhibition upregulated S1PR1 protein expression. Overexpression of S1PR1 robustly promoted Runx2 expression and osteogenic differentiation of BMSCs. Gu Y et al. reported that miR155 inhibits osteogenic differentiation of precursor cells via inhibiting SMAD5 (39). Higashi K et al. reported SMAD1/5/8 as downstream signaling of S1PR1/S1PR2 to induce Runx2 expression in osteoblast (29). Reports from the literature and results of this study indicate that miR155 targets the S1PR1 gene to inhibit Runx2 expression thereby reducing bone regeneration and bone mass.

Since miR155 is upregulated in various cancer including hematological cancers (43). Hematological cancer mainly affects bone marrow that is the dwelling of bone precursor cells. Hematological cancers are associated with bone loss and fracture of vertebrae and long bone. Breast and lung cancer are frequently metastasized to bone and cause osteolysis (51, 52). Cancer/cancer metastasis-induced bone loss-mediated fracture is a serious clinical problem. However, the role of upregulated levels of miR155 on cancer/cancer metastasis-related reduced bone mass is still unclear. Moreover, the prevention of cancer/cancer metastasis-induced bone loss is a huge challenge for clinicians. Since anti-miR155 is already proven to be beneficial for cancer treatment and miR155 knockdown promotes bone regeneration, anti-miR155 could treat cancer as well as caner-induced bone loss as a killing two birds with one stone concept. However, future in vitro and in vivo studies are needed to confirm this hypothesis.

miR155 is overexpressed and plays a key role in the pathophysiology of inflammatory diseases including autoimmune arthritis, osteoarthritis, periodontitis (11, 22, 53). An elevated level of miR155 in arthritis promotes M1 macrophage polarization and inflammation (53). Prevention of bone loss in inflammatory diseases

using currently available therapeutic approaches is not satisfactory. Moreover, inflammation impedes bone regeneration thereby causing the failure of bone tissue engineering approaches. Since anti-miR155 has anti-inflammatory (54) and bone regenerative potential, anti-miR155 could be potential therapeutic to promote bone regeneration even in inflammatory conditions.

This study used both miR155-Tg and miR155-KO mice to investigate the role of miR155 on osteogenesis and bone mass phenotype. Bone regeneration both in ectopic and orthotopic models confirmed the regulatory role of miR155 in bone regeneration. miR155 silenced and S1PR1 overexpressed BMSCs further confirmed the S1PR1 as a target gene of miR155 to regulate Runx2 expression during osteogenesis. The limitation of this study is that we did not analyze the downstream signaling pathway of S1PR1 that regulates Runx2 expression in BMSCS.

miR155 showed a catabolic effect on osteogenesis and bone mass via targeting S1PR1. Our results suggest miR155 as a potential target to promote bone regeneration and higher bone mass. Since miR155 is overexpressed in inflammatory diseases and anti-miR155 has shown anti-inflammatory potential, the miR155 inhibitors could be potential therapeutics to promote bone regeneration even in inflammatory conditions.

Materials and methods

Mice

miR155-KO mice were purchased from the Jackson Laboratory (Stock No. 007745). miR155-Tg mice were constructed as described in our previous reports (55). The C57BL/6J wildtype mice, as the control mice of miR155-KO mice, were purchased from Guangdong medical laboratory animal center. While the FVB mice were littermate control of miR155-Tg mice. The blinded evaluation was used for mice assignments and analysis. The animal experiment was conducted in accordance with the guidelines approved by the Institutional Animal Care and Use Committee of the First Affiliated Hospital of Guangzhou Medical University, Guangzhou, China (2017-078).

320

321 **Bone phenotype analysis**

322 Bone phenotype analysis was performed in 8 weeks old male mice (8 mice/group)
323 using micro-CT. Mice were anesthetized using isoflurane (RWD life science CO.,
324 China), followed by cervical dislocation. Femur with distal growth plate was collected
325 and fixed in 10% buffered formalin. micro-CT scanning was performed to evaluate
326 bone phenotype using Bruker Sky1172 Skyscan (Kontich, Belgium). A total of 100
327 slices (1 mm) below the distal growth plate of the femurs was measured for 3D
328 reconstruction and quantification of trabecular bone as described previously (56). The
329 X-ray tube was operated at 96 kV and 65 μA using a 0.5 mm Al filter with a
330 resolution of 7.93 μm pixels. Scanning was performed by 180° rotation around the
331 vertical axis, camera exposure time of 1300 ms, rotation step of 0.6°, frame averaging
332 of 2, and random movement of 10. 3D images were made using CTvox software
333 (Skyscan, Kontich, Belgium). Data viewer software (Skyscan, Kontich, Belgium) was
334 used for images and linear analysis. Relative bone formation parameters including
335 bone volume/total volume (BV/TV), bone mineral density (BMD), trabecular number
336 (Tb.N), trabecular thickness (Tb.Th), and trabecular separation (Tb.Sp) were
337 analyzed.

338

339 **Ectopic grafting of collagen membrane**

340 Collagen membrane ZH-BIO (China) with 5 mm diameter and 1 mm thickness were
341 osteogenically functionalized by loading 10 μL of 0.3 mg/mL BMP2 solution.
342 BMP2-loaded collagen membranes were implanted in the subcutaneous pockets of
343 miR155-Tg, miR155-KO, and respective control mice. Eight-week-old male mice
344 with 20-22 g body weight (4 mice/group, 1 membranes/mouse) were used for this
345 study. The subcutaneous transplantation of collagen membrane was performed as
346 described previously (57). After 18 days of transplantation, mice were euthanized by
347 isoflurane, collagen membrane was collected, and further analyzed for newly formed
348 bone using micro-CT.

Mice calvaria bone defect healing

Eight-week-old male mice with 20-22 g body weight (3 mice/group, 2 defects/mouse) were used for the calvaria bone defect healing study. The calvaria bone defects model was established as previous reports (58, 59). Surgery was performed under anesthesia with pentobarbital sodium (50 mg/kg) and the body temperature was maintained at 37℃ with a heated platform. After exposure of the cranium surface through a skin incision, a circular and full-thickness bone defect with a 1 mm diameter was generated across the two sides of the sagittal suture using a trephine drill. The bone fragments were taken out. After gentamicin flushing, the incisions were sewed up. After 1 month, the calvaria bones were collected and the healing level was analyzed by micro-CT.

The isolation of primary BMSCs

Euthanized transgenic mice and control male mice (5-6 weeks old) were immersed into 75% ethanol for 5 min. The femurs and tibia were acquired. Primary BMSCs were isolated and expanded as described previously (60). In brief, bone marrow was flushed out from the tibia and femurs and disturbed into small pieces. Cells were collected by centrifugation and plated into flasks and allowed to adhere for 24 h. Nonadherent cells were washed, and culture was continued in DMEM supplemented with 10% non-heat inactivated FBS and 1% penicillin/streptomycin. The cells were cultured in a 5% CO_2 incubator maintaining a humid atmosphere. Cells were trypsinized from 80% confluent culture and passaged. The primary BMSCs in passages 1-3 were used throughout the study.

Analysis of target gene of miR155

TargetScan software was used to predict the target gene of miR155. TargetScan predicted S1PR1 as a possible target gene of miR155.

Plasmid construction and lentivirus preparation

The S1PR1 3'UTR sequences and mutant sequences (200 bp upstream and 200 bp downstream of the binding site from NM_007901.5 transcript) were synthesized and cloned into wildtype plasmid pmirGLO Dual-Luciferase miRNA Target Expression Vector (Promega, USA) by Generay (China). We created S1PR1 3'UTR and S1PR1 mutant 3'UTR plasmids for luciferase assay. The LV242 S1PR1 and control LV242 plasmid were purchased from Genecopedia (USA). miR155 negative control (NC) and miR155 sponge plasmids were purchased from OBIO (China).

For lentiviral transduction, HEK293T cells were co-transfected with expression plasmids (miR155 NC, miR155 sponge, LV242, or LV242 S1PR1) with the packaging plasmids pMD2.VSVG, pMDLg/pRRE, and pRSV-REV using EZ trans transfection regent (Shanghai life iLab BioTechnology Co., LTD, China). After 48 h, fresh lentiviral supernatant was collected and used for infection. BMSCs cells were expanded to 60% confluence prior to lentiviral infection. After infection for 10 h, cells were washed and allowed to recover for 24 h and used for subsequent experiments. miR155 sponge efficacy was analyzed by RT-qPCR. S1PR1 overexpression efficacy was analyzed by western blot analysis.

Luciferase assay

Luciferase assay was performed for further confirmation of S1PR1 as a target gene of miR155. S1PR1 3'UTR (100 ng) with NC (50 nM), S1PR1 3'UTR (100 ng) with miR155 (50 nM), and the S1PR1 mutant 3'UTR plasmid (100 ng) with miR155 (50 nM) were co-transfected into HEK293T cells by lipofectamine 2000 (Thermo Fisher Scientific Inc. USA). After 48 h, the luciferase assay was performed according to the manufacture's instruction using Luc-Pair™ Duo-Luciferase Assay Kit 2.0 (Genecopedia, USA). In brief, the cells were lysed and incubated with 100 μL Fluc work solution for 5 min, the fluorometric measurement was performed by Varioskan® Flash (Thermo Fisher, USA). The lysis solution was added with 100 μL Rluc, incubated for 5 min, and the fluorometric value was measured.

Alizarin red staining

BMSCs (28,000 cells/well) were seeded at 48 well culture plate and cultured with osteogenic medium (50 μg/mL vitamin C, 0.01 μM dexamethasone, and 10 mM β-glycerophosphate). Then the cells were fixed with paraformaldehyde and stained with Alizarin Red S solution (1%, pH 4.2) (Solarbio life sciences, China) for 10 min. The staining was visualized under stereomicroscope Leica EZ4HD (Leica, Germany). For quantitative analysis, the alizarin red-stained mineralized matrix was dissolved with 200 μL 10% hexadecylpyridinium chloride monohydrate for 1 h, and the supernatant was collected. The optical density of the supernatant (100 μL) was measured by a microplate reader at 562 nm.

Immunoblotting

Cells were lysed by using RIPA Buffer (CWBio, China) containing protease inhibitor to extract total protein. Total protein (20 μg) was added to 10% SDS-polyacrylamide gel. The protein was transferred to PVDF membranes (Millipore, USA) after electrophoresis and blocked for 1 h with blocking buffer (Beyotime, China). Then PVDF membranes were incubated with the primary antibodies including ALP (CST, USA, 1:3,000), Runx2 (CST, USA, 1:2,000), S1PR1 (Abcam, UK, 1:2,000), and GAPDH (CST, USA, 1:5,000) overnight at 4℃. The membranes were further incubated with horseradish peroxidase-conjugated secondary antibody for 1 h and reacted with ECL (Millipore, USA). Finally, the photographs were taken by the C-Digit system (Agilent, USA).

RT-qPCR

The microRNAs were extracted from BMSCs with the MolPure® Cell/Tissue miRNA Kit (Yeasen, China) as the manufacture's instructions. The microRNA was further reversed by Tailing reaction using miRNA 1st strand cDNA synthesis kit (Accurate biology, China). In brief, 3.75 μL microRNA, 5 μL 2× miRNA RT Reaction Solution, 1.25 μL miRNA RT Enzyme Mix were incubated at 37℃ for 1 h, 85℃ for 5 min.

RT-qPCR was performed using SYBR® Green Premix Pro Taq HS qPCR Kit (Accurate biology, China) on an AriaMx Real-time quantitative PCR machine (Agilent, USA). The PCR reaction conditions were 95℃ for 30 s, followed by 40 cycles at 95℃ for 5 s and 60℃ for 30 s. The fold change relative to the control group was measured by the $2^{-\Delta\Delta Ct}$ method. The primer used for miR155 detection was TAATGCTAATTGTGATAGGGGT.

Prestoblue cell viability assay

Cell viability was analyzed using PrestoBlue™ cell viability reagent (Thermo Fisher, USA). BMSCs ($4x10^3$ cells/well) were seeded into 96 well culture plates. After 1, 3, and 5 days, the medium was removed and replaced with a cell viability detection medium according to the manufacturer's instructions. After 2 h, the OD value was measured by a microplate reader at 570 nm with a reference wavelength of 600 nm.

Statistical analysis

Data are expressed as mean±SD. Statistical analysis was performed with t-tests for comparison of two groups. $p<0.05$ was considered as a significant difference.

Acknowledgments

This project was funded by National Natural Science Foundation of China (82150410451), the General Guiding Project of Guangzhou (20201A011105), the Medical Scientific Research Foundation of Guangdong Province (B2020027), the Undergraduate Science and Technology Innovation Project of Guangzhou Medical University (2020A049), and High-level University Construction Funding of Guangzhou Medical University (02-412-B205002-1003017 and 06-410-2106035).

Competing interest

All authors declare no conflict of interests.

Data availability

Source data files have been provided for Figures 1-7 as Figure 1 source data-1, Figure 2 source data-2, Figure 3 source data-3, Figure 4 source data-4, Figure 5 source data-5, Figure 6 source data-6, Figure 7 source data-7. And the the western blot raw data was provided as source data-8.

References

1. Gareev I, Beylerli O, Yang G, Sun JX, Pavlov V, Izmailov A, et al. The current state of MiRNAs as biomarkers and therapeutic tools. Clin Exp Med. 2020;20(3):349-59.

2. Wang F, Liang R, Tandon N, Matthews ER, Shrestha S, Yang J, et al. H19X-encoded miR-424(322)/-503 cluster: emerging roles in cell differentiation, proliferation, plasticity and metabolism. Cell Mol Life Sci. 2019;76(5):903-20.

3. Kumar S, Vijayan M, Bhatti JS, Reddy PH. MicroRNAs as Peripheral Biomarkers in Aging and Age-Related Diseases. Prog Mol Biol Transl Sci. 2017;146:47-94.

4. Acunzo M, Romano G, Wernicke D, Croce CM. MicroRNA and cancer--a brief overview. Adv Biol Regul. 2015;57:1-9.

5. Gao Y, Patil S, Qian A. The Role of MicroRNAs in Bone Metabolism and Disease. Int J Mol Sci. 2020;21(17).

6. Wang J, Liu S, Li J, Zhao S, Yi Z. Roles for miRNAs in osteogenic differentiation of bone marrow mesenchymal stem cells. Stem Cell Res Ther. 2019;10(1):197.

7. Elton TS, Selemon H, Elton SM, Parinandi NL. Regulation of the MIR155 host gene in physiological and pathological processes. Gene. 2013;532(1):1-12.

8. Readhead B, Haure-Mirande JV, Mastroeni D, Audrain M, Fanutza T, Kim SH, et al. miR155 regulation of behavior, neuropathology, and cortical transcriptomics in Alzheimer's disease. Acta Neuropathol. 2020;140(3):295-315.

9. Bala S, Csak T, Saha B, Zatsiorsky J, Kodys K, Catalano D, et al. The pro-inflammatory effects of miR-155 promote liver fibrosis and alcohol-induced steatohepatitis. J Hepatol. 2016;64(6):1378-87.

10. Wu Q, Sun S, Li Z, Yang Q, Li B, Zhu S, et al. Tumour-originated exosomal miR-155 triggers cancer-associated cachexia to promote tumour progression. Mol Cancer. 2018;17(1):155.

11. Wu P, Feng J, Wang W. Expression of miR-155 and miR-146a in the saliva of patients with periodontitis and its clinical value. Am J Transl Res. 2021;13(6):6670-7.

12. Shao CC, Yang FM, Qin ZQ, Jing XM, Shu YQ, Shen H. The value of miR-155 as a biomarker for the diagnosis and prognosis of lung cancer: a systematic review with meta-analysis. Bmc Cancer. 2019;19(1).

13. Xin X, Lu Y, Xie S, Chen Y, Jiang X, Song S, et al. miR-155 Accelerates the Growth of Human Liver Cancer Cells by Activating CDK2 via Targeting H3F3A. Mol Ther Oncolytics. 2020;17:471-83.

14. Pasculli B, Barbano R, Fontana A, Biagini T, Di Viesti MP, Rendina M, et al. Hsa-miR-155-5p Up-Regulation in Breast Cancer and Its Relevance for Treatment With Poly[ADP-Ribose] Polymerase 1 (PARP-1) Inhibitors. Front Oncol. 2020;10:1415.

15. Dimitroulas T, Nikas SN, Trontzas P, Kitas GD. Biologic therapies and systemic bone loss in rheumatoid arthritis. Autoimmun Rev. 2013;12(10):958-66.

511 16. S AMEB, Salawu A, Brown JE. Bone Health in Men with Prostate Cancer: Review Article.
512 Curr Osteoporos Rep. 2019;17(6):527-37.
513 17. Kitaura H, Marahleh A, Ohori F, Noguchi T, Shen WR, Qi J, et al. Osteocyte-Related
514 Cytokines Regulate Osteoclast Formation and Bone Resorption. Int J Mol Sci. 2020;21(14).
515 18. Li N, Lee WY, Lin SE, Ni M, Zhang T, Huang XR, et al. Partial loss of Smad7 function
516 impairs bone remodeling, osteogenesis and enhances osteoclastogenesis in mice. Bone.
517 2014;67:46-55.
518 19. Adamopoulos IE. Inflammation in bone physiology and pathology. Curr Opin Rheumatol.
519 2018;30(1):59-64.
520 20. Roodman GD. Biology of osteoclast activation in cancer. J Clin Oncol.
521 2001;19(15):3562-71.
522 21. Kagiya T, Nakamura S. Expression profiling of microRNAs in RAW264.7 cells treated with
523 a combination of tumor necrosis factor alpha and RANKL during osteoclast differentiation. J
524 Periodontal Res. 2013;48(3):373-85.
525 22. Bluml S, Bonelli M, Niederreiter B, Puchner A, Mayr G, Hayer S, et al. Essential Role of
526 MicroRNA-155 in the Pathogenesis of Autoimmune Arthritis in Mice. Arthritis Rheum-Us.
527 2011;63(5):1281-8.
528 23. Arriaga MA, Ding MH, Gutierrez AS, Chew SA. The Application of microRNAs in
529 Biomaterial Scaffold-Based Therapies for Bone Tissue Engineering. Biotechnol J.
530 2019;14(10):e1900084.
531 24. Schmidt T, Schwinge D, Rolvien T, Jeschke A, Schmidt C, Neven M, et al. Th17 cell
532 frequency is associated with low bone mass in primary sclerosing cholangitis. Journal of

533 Hepatology. 2019;70(5):941-53.

534 25. Mann GB, Kang YC, Brand C, Ebeling PR, Miller JA. Secondary causes of low bone mass

535 in patients with breast cancer: a need for greater vigilance. J Clin Oncol. 2009;27(22):3605-10.

536 26. Hsin JP, Lu Y, Loeb GB, Leslie CS, Rudensky AY. The effect of cellular context on

537 miR-155-mediated gene regulation in four major immune cell types. Nat Immunol.

538 2018;19(10):1137-45.

539 27. Xin Q, Li J, Dang J, Bian X, Shan S, Yuan J, et al. miR-155 Deficiency Ameliorates

540 Autoimmune Inflammation of Systemic Lupus Erythematosus by Targeting S1pr1 in Faslpr/lpr

541 Mice. J Immunol. 2015;194(11):5437-45.

542 28. Sato C, Iwasaki T, Kitano S, Tsunemi S, Sano H. Sphingosine 1-phosphate receptor

543 activation enhances BMP-2-induced osteoblast differentiation. Biochem Biophys Res

544 Commun. 2012;423(1):200-5.

545 29. Higashi K, Matsuzaki E, Hashimoto Y, Takahashi-Yanaga F, Takano A, Anan H, et al.

546 Sphingosine-1-phosphate/S1PR2-mediated signaling triggers Smad1/5/8 phosphorylation and

547 thereby induces Runx2 expression in osteoblasts. Bone. 2016;93:1-11.

548 30. Wang Z, Xie Q, Yu Z, Zhou H, Huang Y, Bi X, et al. A regulatory loop containing miR-26a,

549 GSK3beta and C/EBPalpha regulates the osteogenesis of human adipose-derived

550 mesenchymal stem cells. Sci Rep. 2015;5:15280.

551 31. Deng Y, Zhou H, Zou D, Xie Q, Bi X, Gu P, et al. The role of miR-31-modified adipose

552 tissue-derived stem cells in repairing rat critical-sized calvarial defects. Biomaterials.

553 2013;34(28):6717-28.

554 32. Chen A, Wen J, Lu C, Lin B, Xian S, Huang F, et al. Inhibition of miR1555p attenuates the

555 valvular damage induced by rheumatic heart disease. Int J Mol Med. 2020;45(2):429-40.

556 33. Xie Q, Wang Z, Zhou H, Yu Z, Huang Y, Sun H, et al. The role of miR-135-modified

557 adipose-derived mesenchymal stem cells in bone regeneration. Biomaterials. 2016;75:279-94.

558 34. Eskildsen T, Taipaleenmäki H, Stenvang J, Abdallah BM, Ditzel N, Nossent AY, et al.

559 MicroRNA-138 regulates osteogenic differentiation of human stromal (mesenchymal) stem

560 cells in vivo. Proceedings of the National Academy of Sciences of the United States of

561 America. 2011;108(15):6139-44.

562 35. Xie Q, Wei W, Ruan J, Ding Y, Zhuang A, Bi X, et al. Effects of miR-146a on the

563 osteogenesis of adipose-derived mesenchymal stem cells and bone regeneration. Sci Rep.

564 2017;7:42840.

565 36. Li KC, Lo SC, Sung LY, Liao YH, Chang YH, Hu YC. Improved calvarial bone repair by

566 hASCs engineered with Cre/loxP-based baculovirus conferring prolonged BMP-2 and

567 MiR-148b co-expression. J Tissue Eng Regen Med. 2017;11(11):3068-77.

568 37. Yeh CH, Jin L, Shen F, Balian G, Li XJ. miR-221 attenuates the osteogenic differentiation

569 of human annulus fibrosus cells. Spine J. 2016;16(7):896-904.

570 38. Tome M, Lopez-Romero P, Albo C, Sepulveda JC, Fernandez-Gutierrez B, Dopazo A, et

571 al. miR-335 orchestrates cell proliferation, migration and differentiation in human

572 mesenchymal stem cells. Cell Death Differ. 2011;18(6):985-95.

573 39. Gu Y, Ma L, Song L, Li X, Chen D, Bai X. miR-155 Inhibits Mouse Osteoblast

574 Differentiation by Suppressing SMAD5 Expression. Biomed Res Int. 2017;2017:1893520.

575 40. Liu H, Zhong L, Yuan T, Chen S, Zhou Y, An L, et al. MicroRNA-155 inhibits the

576 osteogenic differentiation of mesenchymal stem cells induced by BMP9 via downregulation of

577 BMP signaling pathway. International journal of molecular medicine. 2018;41(6):3379-93.

578 41. Qu B, He J, Zeng Z, Yang H, Liu Z, Cao Z, et al. MiR-155 inhibition alleviates suppression
579 of osteoblastic differentiation by high glucose and free fatty acids in human bone marrow
580 stromal cells by upregulating SIRT1. Pflugers Arch. 2020;472(4):473-80.

581 42. Kardani A, Yaghoobi H, Alibakhshi A, Khatami M. Inhibition of miR-155 in MCF-7 breast
582 cancer cell line by gold nanoparticles functionalized with antagomir and AS1411 aptamer. J
583 Cell Physiol. 2020;235(10):6887-95.

584 43. Witten L, Slack FJ. miR-155 as a novel clinical target for hematological malignancies.
585 Carcinogenesis. 2020;41(1):2-7.

586 44. Yan H, Zhou M, Bhattarai U, Song YB, Zheng MM, Cai JF, et al. Cyclic Peptidomimetics
587 as Inhibitor for miR-155 Biogenesis. Mol Pharmaceut. 2019;16(2):914-20.

588 45. Khalife J, Radomska HS, Santhanam R, Huang X, Neviani P, Saultz J, et al.
589 Pharmacological targeting of miR-155 via the NEDD8-activating enzyme inhibitor MLN4924
590 (Pevonedistat) in FLT3-ITD acute myeloid leukemia. Leukemia. 2015;29(10):1981-92.

591 46. Woeller CF, Roztocil E, Hammond C, Feldon SE. TSHR Signaling Stimulates Proliferation
592 Through PI3K/Akt and Induction of miR-146a and miR-155 in Thyroid Eye Disease Orbital
593 Fibroblasts. Invest Ophthalmol Vis Sci. 2019;60(13):4336-45.

594 47. Wang Y, Zheng ZJ, Jia YJ, Yang YL, Xue YM. Role of p53/miR-155-5p/sirt1 loop in renal
595 tubular injury of diabetic kidney disease. J Transl Med. 2018;16(1):146.

596 48. Hawez A, Al-Haidari A, Madhi R, Rahman M, Thorlacius H. MiR-155 Regulates
597 PAD4-Dependent Formation of Neutrophil Extracellular Traps. Front Immunol. 2019;10:2462.

598 49. Li P, Weng Z, Li P, Hu F, Zhang Y, Guo Z, et al. BATF3 promotes malignant phenotype of

599 colorectal cancer through the S1PR1/p-STAT3/miR-155-3p/WDR82 axis. Cancer Gene Ther.
600 2021;28(5):400-12.
601 50. Okoye IS, Czieso S, Ktistaki E, Roderick K, Coomes SM, Pelly VS, et al. Transcriptomics
602 identified a critical role for Th2 cell-intrinsic miR-155 in mediating allergy and antihelminth
603 immunity. Proc Natl Acad Sci U S A. 2014;111(30):E3081-90.
604 51. Pang Y, Fu Y, Li C, Wu Z, Cao W, Hu X, et al. Metal-Organic Framework Nanoparticles
605 for Ameliorating Breast Cancer-Associated Osteolysis. Nano Lett. 2020;20(2):829-40.
606 52. Cheng X, Wei J, Ge Q, Xing D, Zhou X, Qian Y, et al. The optimized drug delivery
607 systems of treating cancer bone metastatic osteolysis with nanomaterials. Drug Deliv.
608 2021;28(1):37-53.
609 53. Li GS, Cui L, Wang GD. miR-155-5p regulates macrophage M1 polarization and
610 apoptosis in the synovial fluid of patients with knee osteoarthritis. Exp Ther Med.
611 2021;21(1):68.
612 54. Teng C, Lin C, Huang F, Xing X, Chen S, Ye L, et al. Intracellular codelivery of
613 anti-inflammatory drug and anti-miR 155 to treat inflammatory disease. Acta Pharm Sin B.
614 2020;10(8):1521-33.
615 55. Lin X, Qin Y, Jia J, Lin T, Lin X, Chen L, et al. MiR-155 Enhances Insulin Sensitivity by
616 Coordinated Regulation of Multiple Genes in Mice. PLoS Genet. 2016;12(10):e1006308.
617 56. Moussa FM, Cook BP, Sondag GR, DeSanto M, Obri MS, McDermott SE, et al. The role
618 of miR-150 regulates bone cell differentiation and function. Bone. 2021;145:115470.
619 57. Huang H, Feng J, Wismeijer D, Wu G, Hunziker EB. Hyaluronic Acid Promotes the
620 Osteogenesis of BMP-2 in an Absorbable Collagen Sponge. Polymers (Basel). 2017;9(8).

621 58. Li J, Wang T, Li C, Wang Z, Wang P, Zheng L. Sema3A and HIF1alpha co-overexpressed
622 iPSC-MSCs/HA scaffold facilitates the repair of calvarial defect in a mouse model. J Cell
623 Physiol. 2020;235(10):6754-66.
624 59. Reyes R, Rodriguez JA, Orbe J, Arnau MR, Evora C, Delgado A. Combined sustained
625 release of BMP2 and MMP10 accelerates bone formation and mineralization of calvaria critical
626 size defect in mice. Drug Deliv. 2018;25(1):750-6.
627 60. Soleimani M, Nadri S. A protocol for isolation and culture of mesenchymal stem cells from
628 mouse bone marrow. Nat Protoc. 2009;4(1):102-6.

629
630
631
632
633
634
635
636
637
638

639 **Figure legends**

640 **Figure 1.** miR155-Tg mice showed a low bone mass phenotype. (A) Representative
641 micro-CT images. (B) BV/TV, (C) BMD, (D) Tb.N, (E) Tb.Th, and (F) Tb.Sp analysis.
642 Data are presented as mean±SD ,n=8. Significant difference compared to control mice,
643 *p<0.05, **p<0.01.
644 **Figure 2.** miR155-KO mice showed a high bone mass phenotype. (A) Representative
645 micro-CT images. (B) BV/TV, (C) BMD, (D) Tb.N, (E) Tb.Th, and (F) Tb.Sp analysis.
646 Data are presented as mean±SD , n=8. Significant difference compared to control

group, *p<0.05, **p<0.01, ***p<0.001.

Figure 3. Ectopic bone regeneration was inhibited in miR155-Tg mice but enhanced in miR155-KO mice. (A) Representative micro-CT images. (B) BV/TV, (C) Tb.N, (D) Tb.Th, and (E) Tb.Sp analysis. Data are presented as mean±SD , n=4. Significant difference compared to control group, *p<0.05, ***p<0.001.

Figure 4. A higher degree of bone regeneration was observed in the calvarial defect of miR155-KO mice. (A) Representative micro-CT images. (B) BV/TV, (C) Tb.N, (D) Tb.Th, and (E) Tb.Sp analysis. Data are presented as mean±SD , n=6. Significant difference compared to control mice, *p<0.05, **p<0.01.

Figure 5. BMSCs from miR155-Tg mice exhibited compromised osteogenic differentiation. (A) ARS images stained at day 10 of culture, (B) ARS quantification, and (C) Western blot analysis of osteogenic markers. BMSCs from miR155-KO mice showed robust osteogenic differentiation potential. (D) ARS images stained at day 10 of culture, (E) ARS quantification, and (F) Western blot analysis of osteogenic markers. Data are presented as mean±SD, n=4. Significant difference compared to control mice, ***p<0.001, ****p<0.0001.

Figure 6. miR155 silenced BMSCs showed higher osteogenic differentiation potential. (A) ARS images stained at 21 days of culture, (B) ARS quantification, (C) miR155 expression level, (D) cell viability, and (E) Western blot analysis. Data are presented as mean±SD. Significant difference compared to negative control, ***p<0.001, ****p<0.0001. NC: negative control.

Figure 7. miR155 targets S1PR1 to regulate osteogenic differentiation of BMSCs. (A) The TargetScan prediction of miR155 binding site in S1PR1 gene. (B) Luciferase assay, (C) S1PR1 protein expression in BMSCs, (D) ARS images stained at 21 days of culture, (E) ARS quantification, (F) Western blot analysis of osteogenic markers, and (G) cell viability. Data are presented as mean±SD. Significant difference compared to negative control, *p<0.05, **p<0.001.

Figure 8. Scheme of miR155-mediated regulation of osteogenesis. S1P activates the

675 S1PR1, further increasing Runx2 expression to regulate the osteogenic differentiation
676 of MSCs into osteoblasts. Finally, activation of S1PR1 signaling increases the bone
677 mass and may be used as repair of bone defects. miR155 inhibits the process by direct
678 binding with 3'UTR S1PR1 mRNAs. MSCs: mesenchymal stromal cells.

679

680

681

682

683

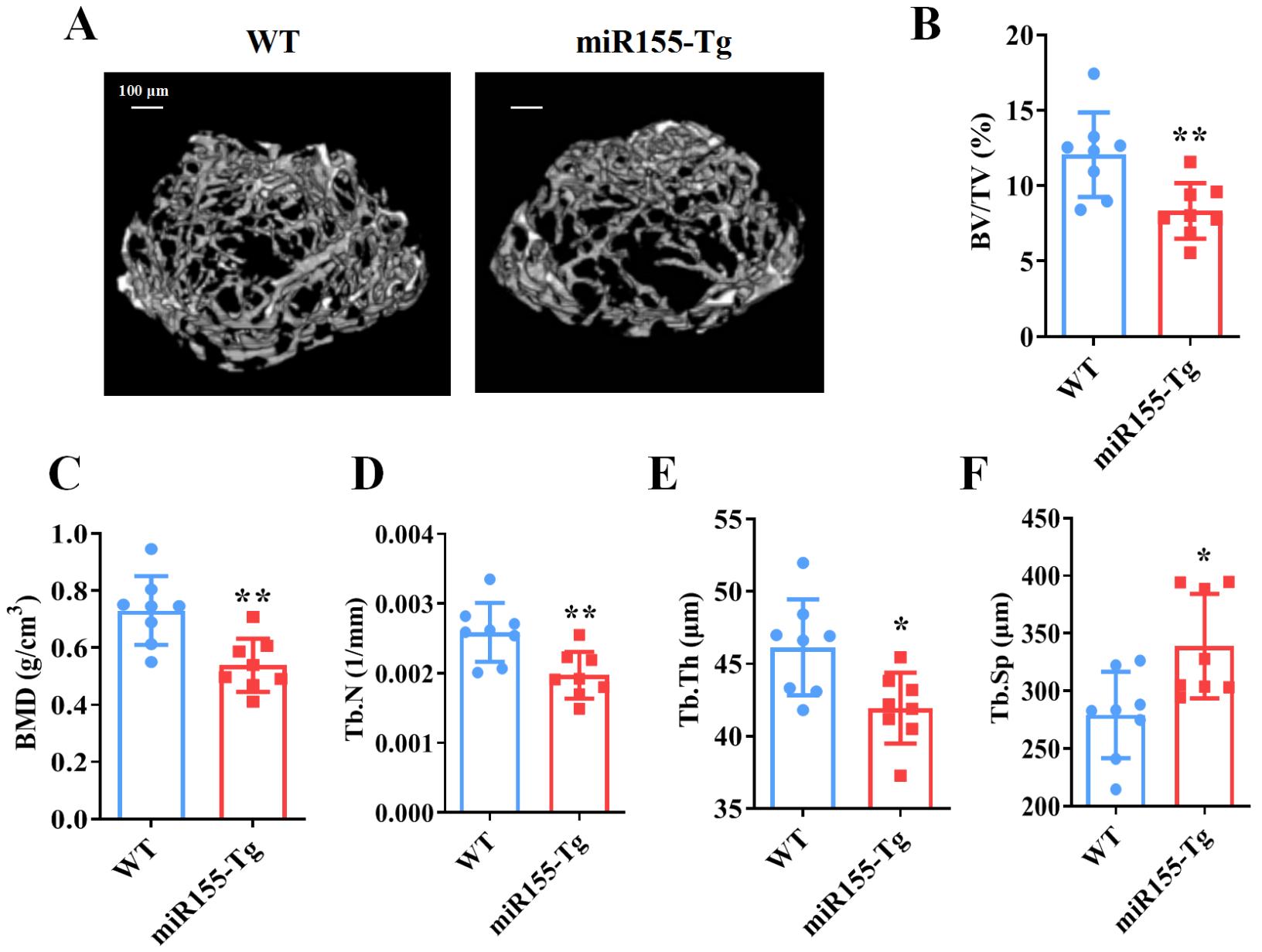
A
WT
miR155-Tg
100 μm
B
BV/TV (%)
20
15
10
5
0
**
WT
miR155-Tg
C
BMD (g/cm3)
1.0
0.8
0.6
0.4
0.2
0.0
**
WT
miR155-Tg
D
Tb.N (1/mm)
0.004
0.003
0.002
0.001
0.000
**
WT
miR155-Tg
E
Tb.Th (μm)
55
50
45
40
35
*
WT
miR155-Tg
F
Tb.Sp (μm)
450
400
350
300
250
200
*
WT
miR155-Tg

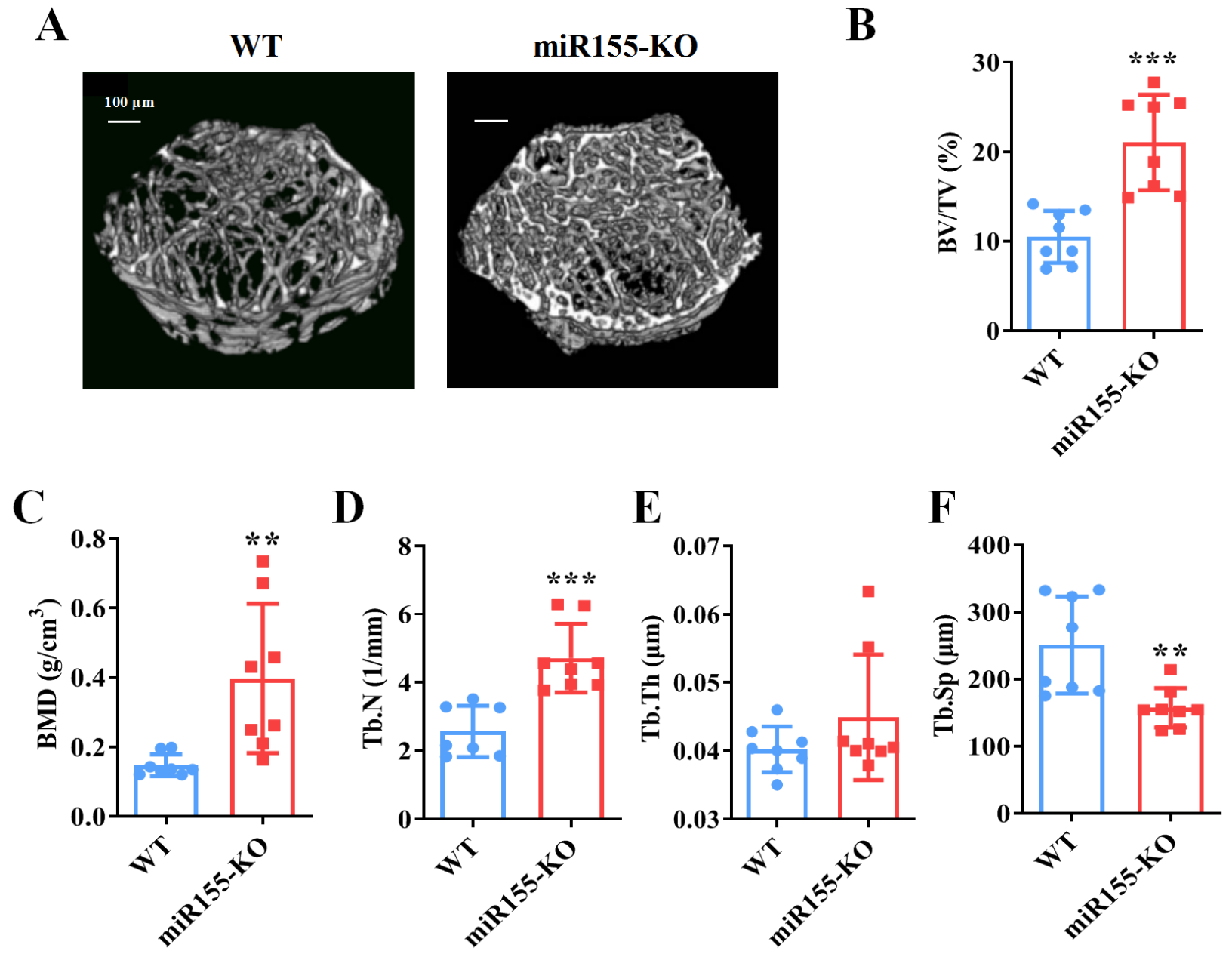
A
WT
miR155-KO
100 μm
B
BV/TV (%)
30
20
10
0
***
WT
miR155-KO
C
BMD (g/cm3)
0.8
0.6
0.4
0.2
0.0
**
WT
miR155-KO
D
Tb.N (1/mm)
8
6
4
2
0
***
WT
miR155-KO
E
Tb.Th (μm)
0.07
0.06
0.05
0.04
0.03
WT
miR155-KO
F
Tb.Sp (μm)
400
300
200
100
0
**
WT
miR155-KO

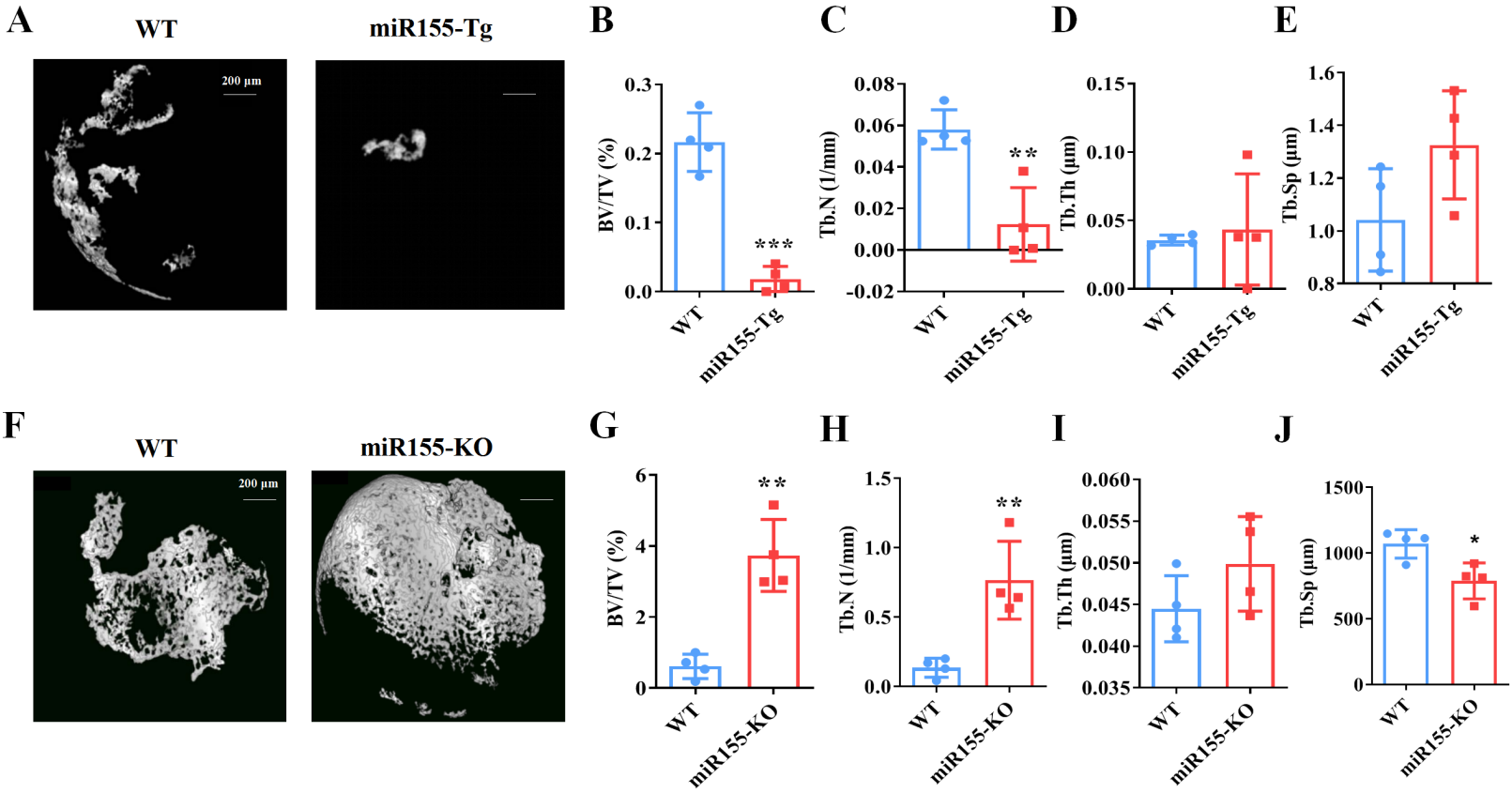
A
WT
miR155-Tg
200 μm
B
BV/TV (%)
0.3
0.2
0.1
0.0
***
WT
miR155-Tg
C
Tb.N (1/mm)
0.08
0.06
0.04
0.02
0.00
-0.02
**
WT
miR155-Tg
D
Tb.Th (μm)
0.15
0.10
0.05
0.00
WT
miR155-Tg
E
Tb.Sp (μm)
1.6
1.4
1.2
1.0
0.8
WT
miR155-Tg
F
WT
miR155-KO
200 μm
G
BV/TV (%)
6
4
2
0
**
WT
miR155-KO
H
Tb.N (1/mm)
1.5
1.0
0.5
0.0
**
WT
miR155-KO
I
Tb.Th (μm)
0.060
0.055
0.050
0.045
0.040
0.035
WT
miR155-KO
J
Tb.Sp (μm)
1500
1000
500
0
*
WT
miR155-KO

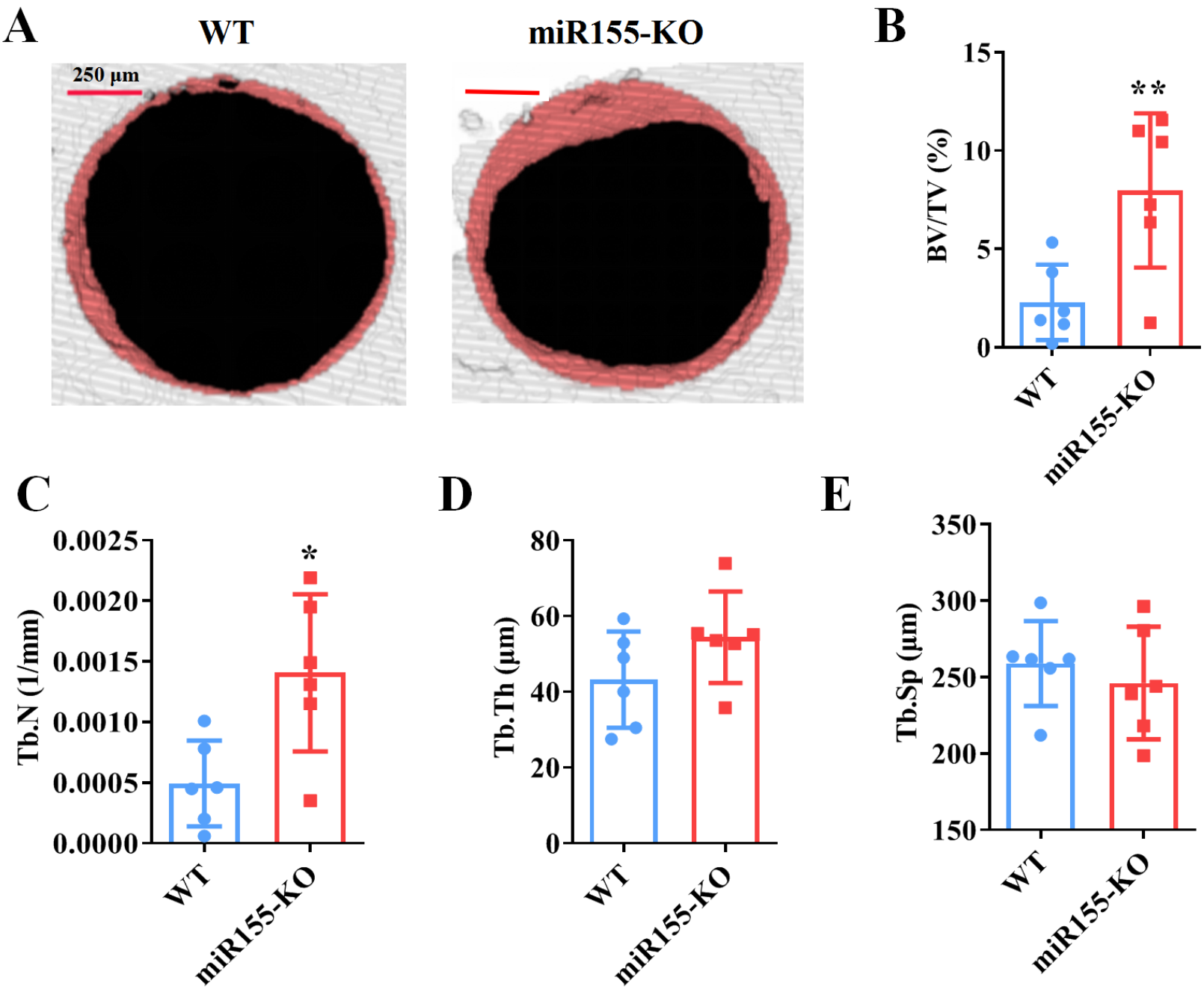
A
WT
miR155-KO
250 μm
B
BV/TV (%)
15
10
5
0
**
WT
miR155-KO
C
Tb.N (1/mm)
0.0025
0.0020
0.0015
0.0010
0.0005
0.0000
*
WT
miR155-KO
D
Tb.Th (μm)
80
60
40
20
0
WT
miR155-KO
E
Tb.Sp (μm)
350
300
250
200
150
WT
miR155-KO

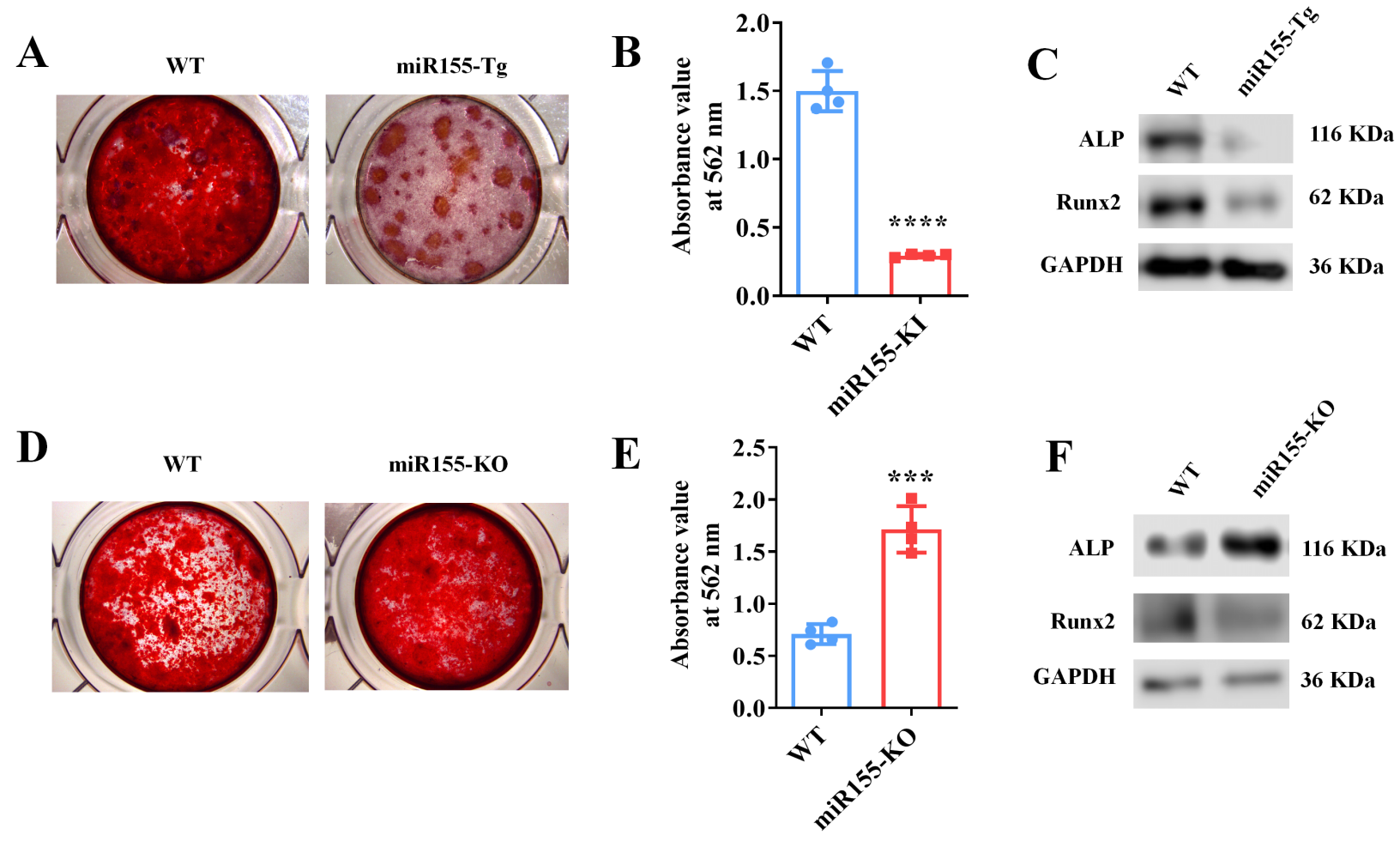
A
WT
miR155-Tg
B
Absorbance value at 562 nm
2.0
1.5
1.0
0.5
0.0
****
WT
miR155-KI
C
WT
miR155-Tg
ALP
116 KDa
Runx2
62 KDa
GAPDH
36 KDa
D
WT
miR155-KO
E
Absorbance value at 562 nm
2.5
2.0
1.5
1.0
0.5
0.0
***
WT
miR155-KO
F
WT
miR155-KO
ALP
116 KDa
Runx2
62 KDa
GAPDH
36 KDa

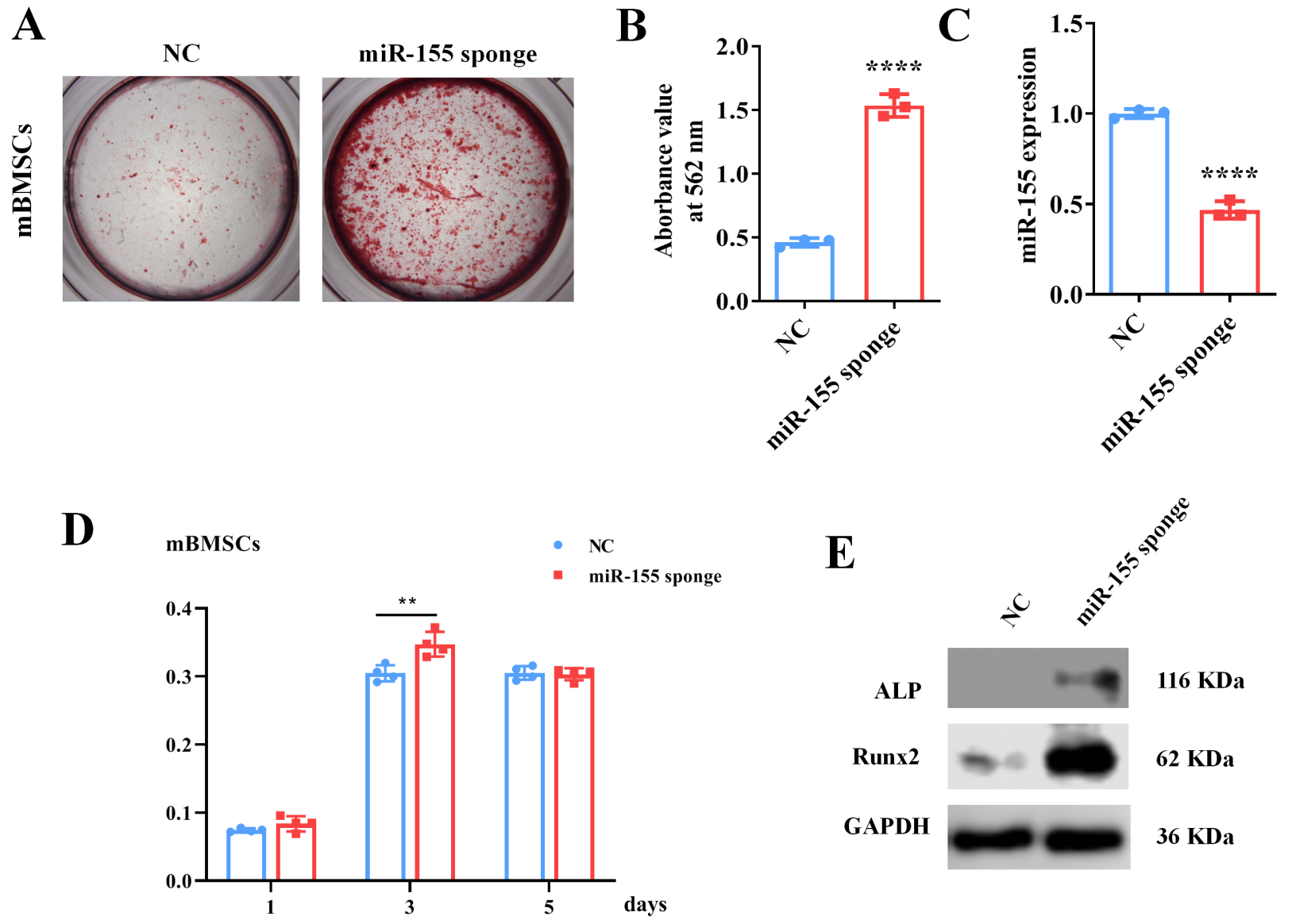
A
NC
miR-155 sponge
mBMSCs
B
Aborbance value at 562 nm
2.0
1.5
1.0
0.5
0.0
****
NC
miR-155 sponge
C
miR-155 expression
1.5
1.0
0.5
0.0
****
NC
miR-155 sponge
D
mBMSCs
NC
miR-155 sponge
0.4
0.3
0.2
0.1
0.0
**
1
3
5
days
E
NC
miR-155 sponge
ALP
116 KDa
Runx2
62 KDa
GAPDH
36 KDa

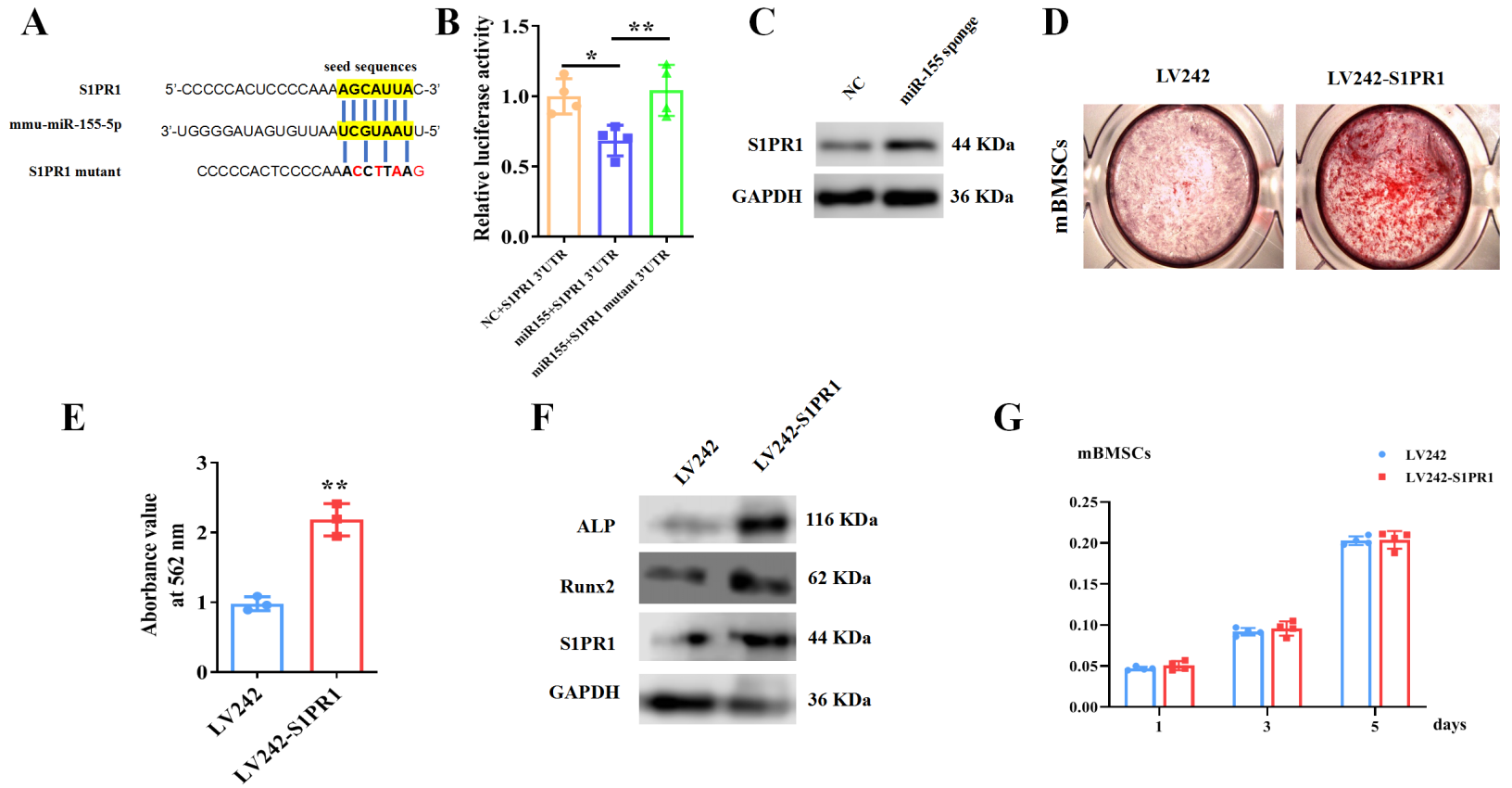
A
seed sequences
S1PR1
5'-CCCCCACUCCCCAAAAGCAUUAC-3'
mmu-miR-155-5p
3'-UGGGGAUAGUGUUAAUCGUAAUU-5'
S1PR1 mutant
CCCCCACTCCCCAAACCTTAAG
B
Relative luciferase activity
1.5
1.0
0.5
0.0
*
**
NC+S1PR1 3'UTR
miR155+S1PR1 3'UTR
miR155+S1PR1 mutant 3'UTR
C
NC
miR-155 sponge
S1PR1
44 KDa
GAPDH
36 KDa
D
LV242
LV242-S1PR1
mBMSCs
E
Aborbance value at 562 nm
3
2
1
0
**
LV242
LV242-S1PR1
F
LV242
LV242-S1PR1
ALP
116 KDa
Runx2
62 KDa
S1PR1
44 KDa
GAPDH
36 KDa
G
mBMSCs
LV242
LV242-S1PR1
0.25
0.20
0.15
0.10
0.05
0.00
1
3
5
days

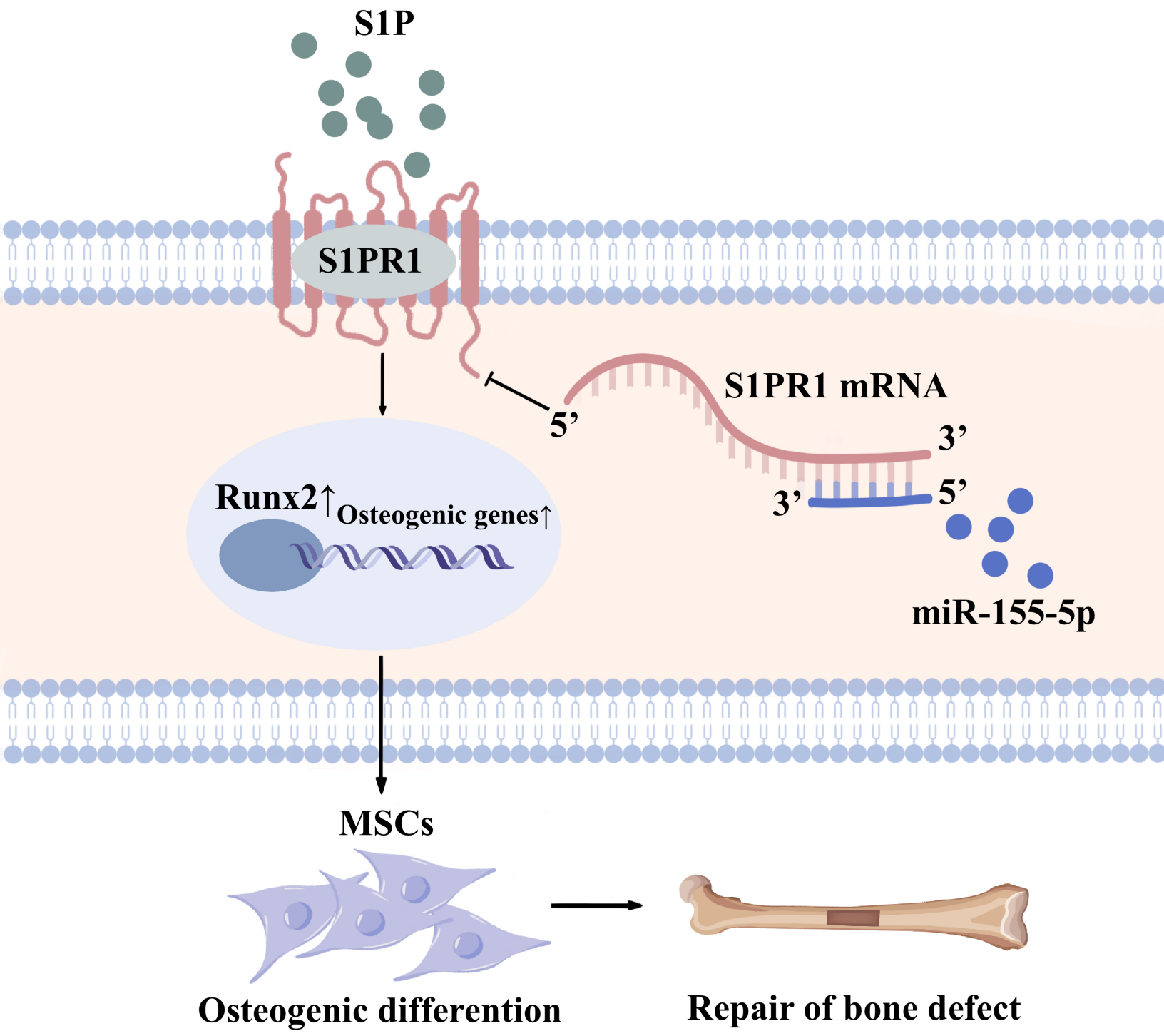
S1P
S1PR1
S1PR1 mRNA
5’
3’
3’
5’
miR-155-5p
Runx2↑Osteogenic genes↑
MSCs
Osteogenic differention
Repair of bone defect